

A Highly Integrated Ka Band Front-End Receiver

Ghulam Mehdi, Hu Anyong and Jungang Miao

School of Electronic and Information Engineering, Beihang University
Beijing,100191, China

Abstract

A highly integrated Ka band front-end receiver is presented. The proposed front-end receiver is developed for a Ka band passive imaging system. The design adopts single-stage heterodyne architecture at 2 GHz intermediate frequency (IF). Further, a two-layer planar technology is adopted for compact realization. The top layer of the front-end comprises of two monolithic microwave integrated circuit (MMIC) low noise amplifiers (LNAs), image rejection bandpass filter (BPF), passive mixer, local oscillator (LO) multiplier chain with associated filters for harmonic rejection, all realized on a single substrate. The bottom layer comprises of IF and power distribution sections. The measured front-end gain, noise figure and image rejection is 40 dB, 4.15 dB and 40 dB respectively. The measured spectral analysis and preliminary system level testing of the front-end exhibits satisfactory performance and confirms the suitability of the proposed front-end for imaging application.

Keywords: Millimeter wave, front-end receiver, passive imaging.

1. Introduction

Passive millimeter wave (MMW) imaging is a method of formation of images through detection of naturally occurring MMW radiation from a scene. The potential advantage of MMW imagers over infrared sensors is the lower attenuation in bad weather conditions such as fog, snow, clouds etc. One of the emerging applications in MMW bands is the passive imaging system for security screening. The concealed hazardous objects and contraband items are potential security threat to human safety. Thus, there is a high demand of low-cost and high performance sensors which could detect hazardous weapons and items. The passive MMW imager is a good choice for such applications. Being inherently non-radiative, passive MMW imagers are safe for the human body scanning. Moreover, such imagers offer sufficient resolution required to detect the location and texture of the concealed objects. Different imaging principles for MMW radiometry are in use. One of the methods is to build such passive imaging system on synthetic aperture interferometric principle. The synthetic aperture interferometric radiometer (SAIR) systems comprise of an antenna-receiver array and a cross-correlator array.

Comparing it with one of its counterpart such as phased array (PA) systems, SAIR acquires all the image pixels in one shot and all the pixels share a longer integration time than PA systems. Consequently, there is less number of receivers in the SAIR systems than PA systems. SAIR system also exhibits larger field of view (FOV) while maintaining the high imaging rate. A typical SAIR imager comprises of an antenna array with corresponding receiving elements and a digital processing unit. The receiving elements are installed on a plane in different possible configurations such as L-shaped, Y-shaped or U-shaped geometry. The digital processing unit computes the visibility function samples and reconstructs the image in real-time [1-3]. The Electromagnetic Engineering Laboratory of Beihang University is engaged in the development of a Ka-band two-dimensional SAIR called BHU-2D [4-5]. The BHU-2D imager is primarily intended for the detection of concealed weapons and contraband items. The proposed front-end receiver is being employed in BHU-2D.

2. Front-end Receiver Architecture

The two receiver configurations usually employed in the MMW radiometer design are the direct-detection (DD) and the super-heterodyne (SH). The DD architecture is a homodyne architecture in which the detector operates at the MMW frequency. The DD receiver architecture does not require a down conversion stage or local oscillator (LO). This reduces the size, power consumption and complexity of the front-end. However, the design of power detectors with high sensitivity such as -50 dBm and moderate dynamic range (typically 10 dB) is hard to realize. The thermal stability of such detectors is also a concern for imaging applications. Moreover, the LNA at MMW frequencies with sufficiently high gain and low noise figure is a challenge as well. In the SH architecture, the MMW frequency is down converted to a much lower intermediate frequency (IF). This is accomplished by mixing the LO with the RF signal. The signal conditioning and detection of this low frequency is much easier than at MMW frequency. The detectors are more readily available and passive components such as filters can be realized

with higher Q. However, consequently, the addition of a mixer and an LO increases the power, size, and complexity of a receiver [6-7]. Over the period of time, various Ka band front-end receivers have been reported. In [8], a substrate integrated waveguide (SIW) filter is employed to reject the image frequency signal. A SIW filter occupies relatively much larger space than the microstrip parallel-coupled filters and such planar structures are not suitable for the applications where space is limited. The front-end module reported in [9] utilizes an active in-phase/quadrature-phase (I/Q) mixer and a 90° hybrid divider to perform image frequency rejection. Image suppression of 15 dB is achieved with this configuration. Such configuration also occupies a large space, the active IQ mixer consumes power and the achieved image rejection is relatively much lower than the typical desired value of 25 dB.

In this work, a MCM level design approach is adopted to realize the proposed low-cost, highly integrated front-end receiver. Single-stage super-heterodyne configuration is employed to reduce the requirement of hardware resources and complexity of the design. Conversely, the design of the image rejection filter becomes more critical as the image lies close to the MMW frequency due to low IF. The specifications of the front-end are tabulated in Table 1. In order to realize the front-end in the given volume, die chips are preferred over an SMT package. This yields compact size and allows a narrow channel with cutoff frequencies higher than the operating frequency band. The front-end receiver block diagram is depicted in Fig.1. For compact realization, a two-layer planar technology is adopted. These two layers have been labeled as a top layer and the bottom layer. The upper layer comprises of active devices and passive structures such as filters, matching networks, operating from 2 GHz to 34 GHz, all realized on a single substrate for seamless integration. The blocks enclosed in the solid line box in Fig.1 depict the top layer. The bottom layer comprises of chip low pass filter (LPF), IF amplifier and step-impedance BPF. The blocks enclosed in the dotted line box in Fig.1 depict the bottom layer. The selection of the substrate is vital in the MMW circuit design and is very specific to the application. Ceramic substrates such as alumina are not considered as such substrates require thin film technology process which results in higher cost. Moreover, at millimeter wave frequencies, very high dielectric constant put stringent machining tolerances and also dimensions of some of the distributed structures may become impractical. A low-cost commercially available PTFE substrate ($\epsilon_r=6.2$, 254 μm thickness) is selected for this work.

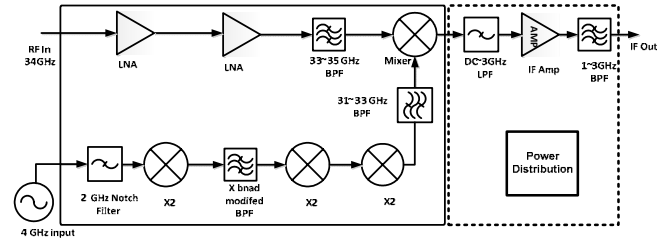


Fig. 1 Block diagram of the Ka-band front-end receiver module.

Table 1: Receiver specifications

Parameter	Specification
Center Frequency	34 GHz
Bandwidth	2 GHz
LO Frequency	32 GHz (used for RF front end)
IF Frequency	2 GHz (used for I/Q demodulator)
Front-end Gain	40 dB
Image Rejection	>30 dB
Noise Figure	4 dB
Volume	120*20*20 mm ³

3. Detailed Design

3.1 Waveguide-to-microstrip transition

A reactively tuned waveguide-to-microstrip transition is adopted because of its simplicity and ease of integration. The other advantage is that the front-end receiver with such kind of transitions can be hermetically sealed later for environmental protection. The transition comprises of a right-angled junction of waveguide and coaxial line, where the center conductor pin of the coaxial line extends through the broad wall into the waveguide and acts as a coupling probe inside. The probe in the waveguide acts as an impedance transformer from the low impedance of the coaxial line, typically 50 Ω , to the high impedance of the waveguide, typically greater than the free space impedance. The match is accomplished by adjusting the back-short distance and the length of the center conductor probe. Since the maximum electric field is at the center of the wide dimension of the waveguide, the probe is placed in the center. The equivalent model of the transition is shown in Fig.2. The right side of the model represents the waveguide by a resistor equal to the waveguide impedance. The transition is represented by a capacitive reactance, in series with the coaxial line. The waveguide is shunted with the equivalent susceptance of the waveguide stub, the left part of the waveguide [10-11].

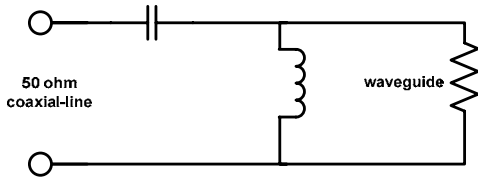


Fig. 2 Waveguide-to-microstrip transition equivalent model.

The coaxial line impedance has to be matched to the frequency dependent waveguide impedance. While looking from the coaxial line at the plane of the waveguide wall, the input impedance Z_i is given by:

$$Z_i = R + jX \quad (1)$$

Where

$$R = \frac{Z_0}{2\pi^2} \frac{\lambda \lambda_g}{ab} \sin^2(2\pi L / \lambda_g) \tan^2(\pi d / \lambda) \quad (2)$$

and

$$X = \frac{Z_0}{4\pi^2} \frac{\lambda \lambda_g}{ab} \tan^2 \frac{\pi d}{\lambda} \left[2X_p + \sin\left(\frac{4\pi L}{\lambda_g}\right) \right] \quad (3)$$

where

L =Back-short distance

d =Length of the probe inside the waveguide

X_p =Reactance of the probe normalized with respect to the waveguide impedance

The initial values of d and L are computed from expressions (1-3) and later the transition is simulated and optimized in the full-wave EM solver. The optimum back-short distance “ L ” is 2.4 mm and pin length “ d ” is 1.4 mm. The simulated and measured input return loss of two front-ends receivers is shown in Fig.3. The deviation in the measured results primarily arises from the bond wire discontinuities and manufacturing tolerances.

3.2 Low noise amplification & image rejection

Passive MMW radio receivers need to be able to detect very weak signals. These signals after detection and amplification are usually down converted to lower intermediate frequencies. From the Ferris’s expression for total noise figure computation, it is well known that the total noise figure of any radio receiver system is primarily determined by the noise temperature of the first stage in the receiver system. Usually, LNA is one of the first components in the system; the overall noise figure of the LNA must be as low as possible. Moreover, the LNA stage needs to provide enough gain to be able to overcome the noise added by the subsequent stages such as a passive lossy mixer in the heterodyne receivers [12].

Commercially available low noise gallium arsenide MMIC LNA die chips are used in the design. The gain requirement at MMW frequency is about 40 dB. Since the amplifiers are to be employed in the propagating cavity, the gain is broken up into two 20 dB gain stages. In order to reduce the non-propagating signal in the channel from the output back to the input, the distance between the two stages is good enough to provide at least 20 dB isolation. This minimizes the gain ripples (less than 0.1 dB) in the passband and prevents amplifiers to go into oscillations.

The BPFs are used in the radio frequency receivers for suppression of the image frequency which results in the improved noise figure. The topology of such filter is very critical for the realization of compact receivers. Over the years, parallel-coupled BPF has remained the most popular topology at MMW bands. Its long-narrow aspect ratio and the ability to be placed axially rotated in the receiving channel makes it the ultimate choice when the space is the primary constraint. Moreover, this type of filter has other advantages such as easy design procedure, wide bandwidth and planar structure. A five stage, all symmetric parallel-coupled BPF is designed, fabricated and tested for image rejection purposes [13-14]. The effects of manufacturing tolerances on the design of the parallel-coupled BPF are investigated. Consequently, a procedure is devised for a first pass design of such filters. The open-end effect in the half-wavelength resonator section is compensated with the round-ended corners rather than decrementing the lengths in a conventional way. The widths of all the half-wavelength resonators are set equal to avoid discontinuities in the interior of the filter. The fabrication tolerances are compensated in the design prior to manufacturing. The Through-Reflect-Line (TRL) calibration method is employed to obtain the de-embedded measured results at the device plane. The measured results are in good agreement with the simulated results as illustrated in Fig.4. The insertion loss is 3 dB, passband variation is less than 1 dB and the filter exhibits 3dB bandwidth of 3.8 GHz.

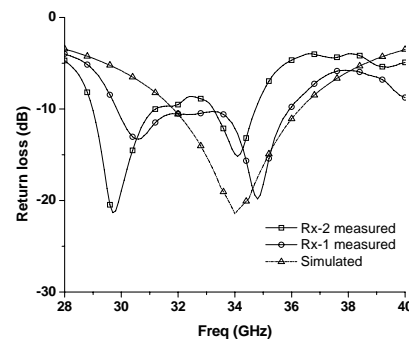


Fig. 3 Simulated and measured return loss of two receivers.

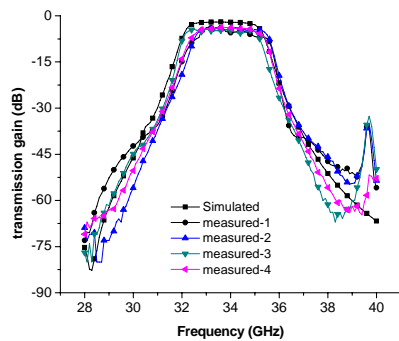


Fig. 4 Simulated and measured response of fabricated IR BPFs.

3.3 Local Oscillator Block

The generation of the local oscillator signal at MMW frequencies with low phase noise and moderate output power is needed to be able to drive the down conversion stage. One of the ways is to generate the MMW frequency signal directly at the fundamental by using a tuned oscillator. However, there are issues associated with this direct generation such as stability, jitter, phase noise and low output power. Alternatively, a MMW signal could be generated employing an up-conversion stage. However, an up-conversion mixer requires high linearity and low noise to minimize the amount of spurious power spread into adjacent channels.

In the presented work, frequency multipliers are employed for the generation of low phase noise local oscillator signal while maintaining the high out power of 15 dBm to drive the down conversion stage. An optimum circuit configuration in terms of space, cost and performance is adopted to transform 4 GHz input signal into 32 GHz LO signal. The block diagram of the LO generation block is shown in Fig.4. The first component in the LO block is a 2 GHz notch filter. The 4 GHz input signal from the frequency synthesizer has a 20 dBc half frequency harmonic component. The 2 GHz notch filter suppresses this half frequency component more than 50 dB. The design of this notch filter is described in section 3.5. The first active doubler converts 4 GHz signal to 8 GHz. A modified parallel-coupled BPF with improved upper sideband suppression follows the active doubler. The detailed design of this filter is described in section 3.4. The subsequent stages comprise of an 8 GHz to 16 GHz passive doubler, 16 GHz to 32 GHz active multiplier and 31~33 GHz band parallel-coupled BPF. The design of 31~33 GHz band parallel-coupled BPF is similar to that of image rejection thus not discussed. This optimum configuration of employing a modified parallel-coupled

BPF with higher upper sideband suppression in conjunction with a subsequent passive doubler mitigates the requirement of 16 GHz intermediate stage BPF for harmonic suppression and results in a compact multi-chip module (MCM).

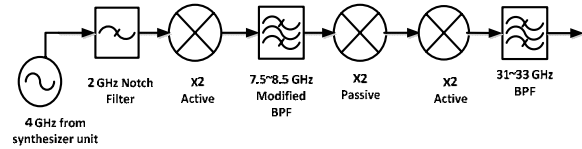


Fig. 5 Block diagram of LO generation unit.

3.4 X-band Modified Band-pass Filter

A modified parallel-coupled BPF with improved upper sideband suppression has been designed, fabricated and tested. After necessary validation, the same has been employed in the LO block of the front-end receiver for the suppression of harmonics generated by the first multiplier stage. The first multiplier being an active component produces strong first (at 4 GHz) and third (at 12 GHz) harmonic components at the output other than the desired 8 GHz signal. The power levels of these harmonic are 20 dBc with respect to the output power of 8GHz signal. These spurs if not filtered out at this stage would deteriorate the receiver performance. The aim is to design a BPF with symmetric frequency response to equally suppress both of these harmonic signals. Parallel-coupled topology is adopted for this filter due to its advantages mentioned earlier in section 3.2. However, parallel-coupled filters when implemented in microstrip have an asymmetric frequency response and also exhibit a spurious passband at twice the center frequency. Due to the asymmetric frequency response, the filter shows steeper roll-off on the low frequency side than on the higher frequency side. This asymmetric response and undesired spurious passband are due to the inhomogeneous dielectric medium surrounding the conductors, which causes the odd-mode wave to propagate faster than the even-mode wave in the coupled microstrip lines. Since the length of each coupled section in a parallel coupled filter is the same for both even and odd modes, the unequal phase velocities of these modes create different half wavelength frequencies for these modes. Contrary to microstrip, in stripline, the medium is homogeneous. This allows the half wavelength frequencies to coincide and so create a zero response at this frequency in Stripline parallel-coupled filters [15-16].

Various methods have been reported for the improvement of the upper stop band rejection and response symmetry of

microstrip parallel-coupled filters. For example in [17], instead of the microstrip open ends in the traditional parallel-coupled filter, there are microstrip gaps in the modified filter and these gaps are of the offset type. By carefully choosing the gap width, one can optimize the stopband rejection and the response symmetry. This method lacks in prescribing straight forward design procedure and is rather iterative. The method proposed in [18] extends the odd mode phase length by allowing the coupled lines to overlap lines outside the resonator. This configuration makes the odd mode length longer than the even mode and thus compensates for the phase velocity difference between the two modes. However, this method significantly increases the filter bandwidth because the coupling of each resonator is increased. Further, according to this design given in [19], the attenuation poles can be obtained at any desired frequency by means of coupling structures. Thus, a filter with excellent attenuation characteristics for various applications can be achieved. However, due to the anti-parallel coupling structure in the design, the filter occupies much larger space and thus not suitable for the application where space is primary constraint. Lately, another interesting method is presented in [20] to suppress the first spurious response of microstrip parallel-coupled filters. Grooves in the substrate are oriented parallel to all coupled lines and just next to them. It is shown that the grooves equalize the even- and odd-mode phase velocities in microstrip coupled lines and, thus suppress the spurious response. The two grooves with proper width and depth are cut along the microstrip coupled lines and just beside them. However, cutting grooves adds extra machining work and the effectiveness of this method may vary from substrate to substrate which have different compositions.

The design of a stripline parallel-coupled BPF with improved upper sideband rejection slope is reported in [21]. In this work, the same concept is adopted to realize parallel-coupled BPF on microstrip. It is well known that in stripline, the conductor is embedded in a homogeneous and isotropic dielectric, and the phase velocity and the characteristic impedance of the dominant mode TEM do not vary with frequency. In the proposed design, each pair of the coupled lines has one section lengthened by an offset δ , while the adjacent section is shortened by the same amount. By introducing such offsets (δ), the transmission line between each J-inverter is preserved as a $\lambda/2$ transmission line resonator. The transmission zero between the fundamental and 1st harmonic can be shifted and controlled by the amount of δ offset. By shifting the transmission zero close to the center frequency of the filter, higher rejection at the desired frequency could be achieved. However, there is one constraint in the design. In order to preserve the half-wavelength resonators in the

parallel-couple filters, this design can only be applied to even order filters. In the modified filter, the transmission zeros occur at the frequency for which the physical lengths of the $90^\circ + \delta$ sections correspond to a half-wavelength where δ is the offset length. This can be written as:

$$L(90^\circ + \delta)_{f_o} = L(180^\circ)_{f_i} \quad (4)$$

where f_i the new frequency at which transmission zero occurs.

In our design, the center frequency is 8 GHz. The third harmonic of the active multiplier lies at 12 GHz. It is computed from expression (4) that for $\delta=30^\circ$, the transmission zero occurs at 12 GHz and results maximum attenuation. Once the offset length is determined, the rest of the design steps are as follows. The element values of a 4th order Chebyshev response filter with 0.01 dB ripple are calculated. The J-Inverter values for the filters are calculated using expressions (5-6). Then, the corresponding even and odd mode impedances for the filters with $\delta=0^\circ$ and $\delta=30^\circ$ have been computed using expressions (7-8). The computed even and odd mode impedances are given in Table 2. A LineCalc tool from Agilent is used to calculate the physical dimensions of the microstrip coupled lines for the two filters. It may be noted that for the Stripline coupled filter design, the circuits with desired passband responses can be exactly synthesized. The values of even-mode impedance, odd-mode impedance, and electrical length for each coupled-line section could be well determined. However, if the same design is realized on microstrip, the values of electrical length are different for even and odd modes [22]. Due to this difference, we have experienced degraded performance of filters in terms of increased reflection, passband variations and relatively higher insertion loss both in simulations as well as in measured results. The layout of the two filters is shown in Fig. 6. The two filters with 0 and 300 offset have been fabricated and tested. The measured versus simulated results of each filter are shown in Fig. 7 and Fig.8. The measured results of two fabricated filters are illustrated in Fig.9 and the measured performance is compared in Table 3. The modified BPF with 30° offset exhibits and improved upper sideband suppression of 16.5 dB when compared with the conventional design with 0° offset.

$$\frac{J_{01}}{Y_0} = \sqrt{\frac{\pi FBW}{2 g_0 g_1}} \quad (5)$$

$$\frac{J_{j,j+1}}{Y_0} = \frac{\pi FBW}{2} \frac{1}{\sqrt{g_j g_{j+1}}} \quad (6)$$

where $j= 1$ to $n-1$

$$Z_{0o} = \left(\frac{1}{Y_0}\right) \frac{1 - \left(\frac{J}{Y_0}\right) \text{Cosec} \theta_c + \left(\frac{J}{Y_0}\right)^2}{1 - \left(\frac{J}{Y_0}\right)^2 \text{Cot}^2 \theta_c} \quad (7)$$

$$Z_{0e} = \left(\frac{1}{Y_0}\right) \frac{1 + \left(\frac{J}{Y_0}\right) \text{Cosec} \theta_c + \left(\frac{J}{Y_0}\right)^2}{1 - \left(\frac{J}{Y_0}\right)^2 \text{Cot}^2 \theta_c} \quad (8)$$

Table 2: Even and odd mode impedances of 0 and 30° offset.

Offset (δ) deg	Z_{01e} Z_{45e}	Z_{01o} Z_{45o}	Z_{12e} Z_{34e}	Z_{12o} Z_{34o}	Z_{3e}	Z_{3o}
0	84.5	37.5	60	43	57	44.5
30	91.3	36.9	61.2	42.3	57.9	44



Fig. 6 Layout of (top) conventional BPF with $\delta=0^\circ$ (bottom) modified BPF with $\delta=30^\circ$

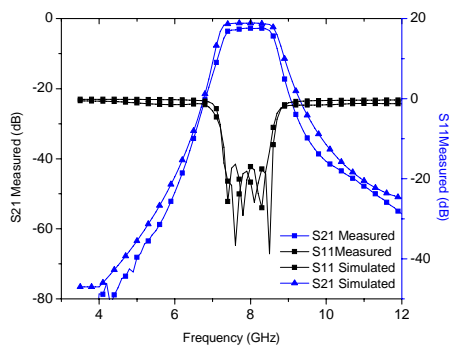


Fig. 7 Simulated and measured response of conventional ($\delta=0$) BPF.

Table 3: Measured results of conventional and modified BPF.

Parameters	Conventional	Modified
Center frequency (GHz)	8	8
Bandwidth (GHz)	1.35	1.4
Insertion loss (dB)	2.7	3.0
Rejection at 5 GHz	-80	80
Rejection at 12 GHz	-55.5	-72

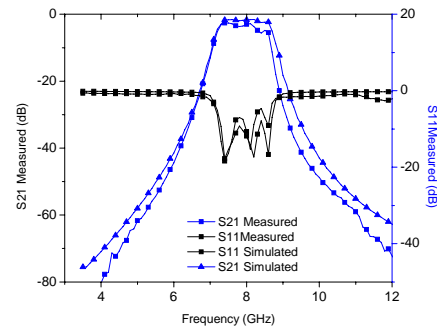


Fig. 8 Simulated and measured response of modified ($\delta=30^\circ$) BPF.

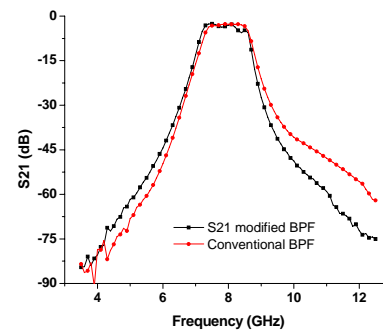


Fig. 9 Comparison of conventional and modified BPFs.

3.4 Notch filter design

The 4 GHz input signal from the synthesizer unit contains 23 dBc half frequency spur. In order to obtain spurious free output spectrum of the front-end receiver, this 2 GHz harmonic needs to be suppressed. A microstrip notch filter with three open-circuited stubs for a FBW = 0.5, centered at 2 GHz frequency is designed. The shunt quarter wavelength open-circuited stubs are separated by unit elements. The unit element is again $\lambda/4$ long at the center stop band frequency [23]. The characteristic impedances for the open-circuited stubs and unit elements are calculated for the desired specifications. The $\lambda/4$ comes out to be 19 mm long and such dimensions could not be accommodated in the available space. One of the options is to realize the filter on a different substrate with a much higher dielectric constant such as 10.8. In order to realize the filter on the same substrate, a meander line structure is adopted as depicted in Fig.10. This scheme significantly reduces the filter size. However, the discontinuities and the coupling effect needs to be considered. The open-end, T-junction and bend effects

have been taken into account to determine the final filter layout. The design is optimized for improved performance with a steeper stopband response. The measured results show the suppression at 2 GHz is more than 55 dB as shown in Fig.11.

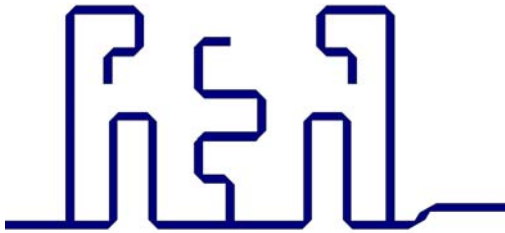


Fig. 10 Meandered line notch filter layout.

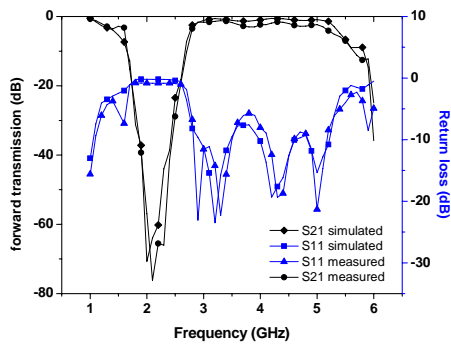


Fig. 11 Meandered line notch filter simulated and measured results.

4. Front-end measurements

The die chips are eutactically attached with the metallic enclosure surface. The bond wire lengths are kept as short as possible. The two front-end receivers are measured on Agilent PNA N5225A. Fig.12 and 13 shows the four fabricated front-end receivers and measurement setup respectively. The measured gain and frequency response of the two receivers along with the simulated one is depicted in Fig.14. The measured gain is 40 dB in the working band of 33-35 GHz. The image rejection is better than 40 dB. The gain and frequency response of the two receivers are in good match. The spectral analysis of the front-end exhibits good spurious free passband spectrum as depicted in Fig.15. The measured noise figure of the two receivers is 4.0 dB and 4.15 dB respectively and are in good agreement with the theoretical one. The breakdown of the theoretical noise figure along with the measured results is given in Table 4.

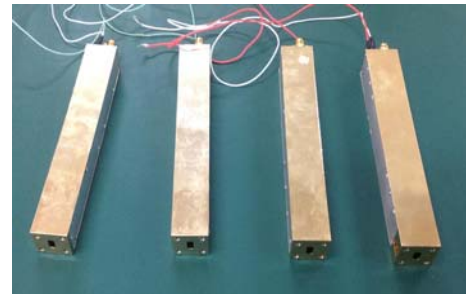


Fig. 12 Fabricated front-end receivers.



Fig. 13 Measurement setup.

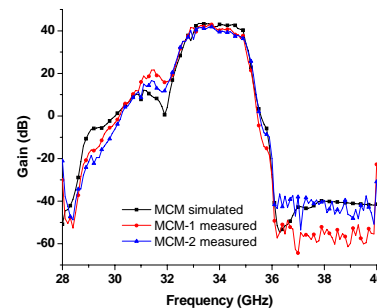


Fig. 14 Measured frequency response of two front-end receivers

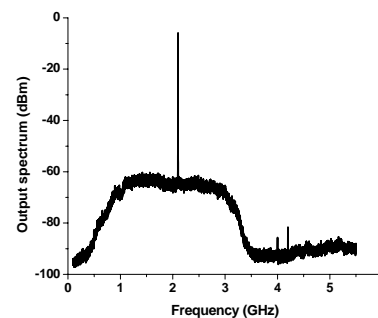


Fig. 15 0.1 GHz-5.5 GHz output spectrum the front-end

Table 4. Comparison of theoretical and measured noise figure

Parameters	Theoretical	Measured)
LNA noise figure (dB)	2.7	4.10
Waveguide-to-microstrip transition loss (dB)	0.7	
50 ohms matched line loss (dB)	0.2	
Total noise figure according to Friis expression (dB)	4.0	

In order to validate the performance of the front-end receivers for imaging applications, a preliminary test setup is established to compute the correlation coefficients. The setup comprises of a matched noise source, variable attenuator, variable phase shifter, two fabricated MMW front-end receivers, IF IQ (In phase- quadrature) receivers and DSP unit. The system level test setup is depicted in Fig.16 (IF IQ receiver and DSP unit not shown). A power divider feeds the noise signal to the two front-end receivers. A variable phase shifter which follows the power divider is introduced in one the receiver path to obtain different correlation coefficients. The IF IQ receiver translates the 2 GHz output signal to 200 MHz IQ baseband signals. Then the baseband signal is sampled in DSP unit and complex correlation coefficients are computed. The correlation coefficient can be tuned by adjusting the phase shifter. Ideally as the phase shifter changes the phase, the real or imaginary part of the complex correlation coefficient should be a cosine curve while in the Cartesian coordinate it corresponds to a circle. Fig.17 illustrates the measurement results which are close to ideal. The gap in the test curve is due to the fact that the phase shifter can only shift the phase up to 280 degrees. Moreover, the circle is not perfect due to the variations in the insertion loss of the phase shifter at different phase angles.

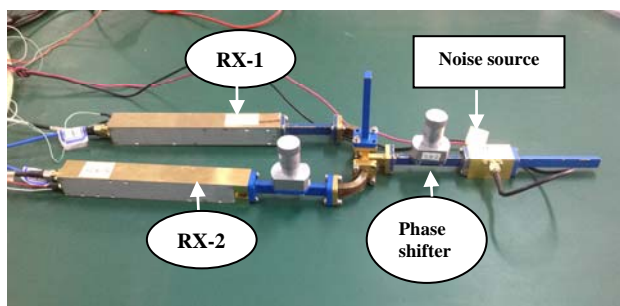
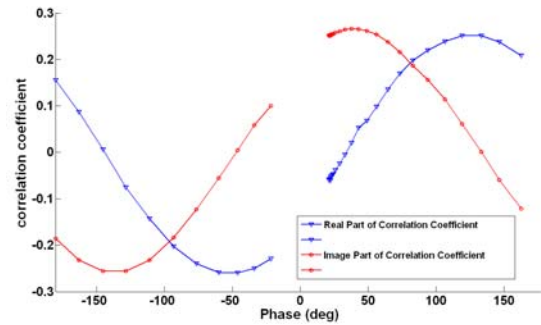


Fig. 16 System level test setup with fabricated two front-end receivers



(a)

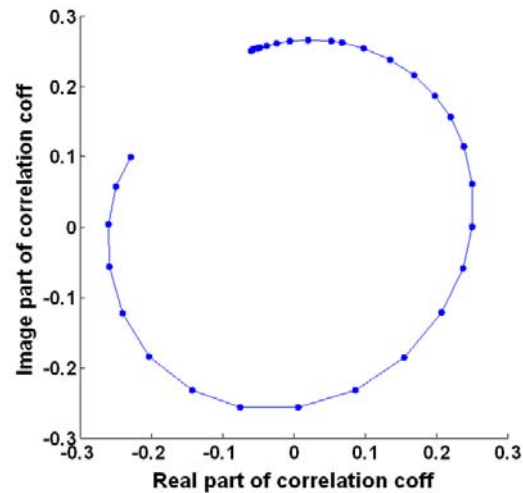


Fig. 17 (a) Complex correlation coefficient cosine curves (b) complex correlation coefficient in the CCS

4. Conclusions

In this paper, a highly integrated Ka band front-end receiver module for a passive Ka band imager is designed, fabricated and tested. All the blocks of the receiver operating from 2 GHz to 34 GHz are realized on a single, low-cost soft substrate employing conventional photolithography process. This provides excellent ease of manufacturability and seamless integration. A five-pole all symmetric parallel-coupled BPF is designed to obtain image rejection better than 40 dB. An X band modified parallel-coupled BPF with improved upper sideband suppression is designed and employed for multiplier harmonic suppression. The upper sideband suppression is at least 16 dB better than its conventional counterpart filter. A compact notch filter with a meander line with mitered bends is designed, fabricated and employed in the receiver. The measured gain and noise figure of the front-end is 40 dB and 4.15 dB respectively.

References

- [1] Salmon, N. A., P. N. Wilkinson, C. T. Taylor, and M. Benyazzar, "Minimising the costs of next generation aperture synthesis passive millimetre wave imagers," *Proc. SPIE*, Vol. 8188, 818808, Oct. 6, 2011.
- [2] Lovberg, J. A., C. Martin, and V. G. Kolinko, "Video-rate passive millimeter-wave imaging using phased arrays," *Proc. MWSYM*, 1689-1692, Honolulu, HI, Jun. 3-8, 2007.
- [3] Oka, Soichi, et al. "Latest trends in millimeter-wave imaging technology." *Progress In Electromagnetics Research Letters* 1 (2008): 197-204.
- [4] Zheng, Cheng, et al. "A Passive Millimeter-Wave Imager Used for Concealed Weapon Detection." *Progress In Electromagnetics Research B* 46 (2013): 379-397.
- [5] Zheng, Cheng, et al. "Closed Form Calibration of 1bit/2level Correlator Used for Synthetic Aperture Interferometric Radiometer." *Progress In Electromagnetics Research M* 29 (2013): 193-205.
- [6] Skou, Neils. "Microwave radiometer systems: design and analysis." Norwood, MA, Artech House, 1989, 171 p. 1 (1989).
- [7] Razavi, Behzad, and Razavi Behzad. *RF microelectronics*. Vol. 1. New Jersey: Prentice Hall, 1998.
- [8] Chen, Jixin, Pinpin Yan, and Wei Hong. "A Ka-band receiver front end module." In *Microwave Conference Proceedings (APMC)*, 2010 Asia-Pacific, pp. 535-537. IEEE, 2010.
- [9] Schreiber, Eric, Simon Anger, and Markus Peichl. "Design of an integrated Ka band receiver module for passive microwave imaging systems." In *Semiconductor Conference Dresden (SCD)*, 2011, pp. 1-4. IEEE, 2011.
- [10] Delmotte, Peter. "Waveguide-coaxial line transitions." *Belgian Microwave Roundtable* (2001).
- [11] Keam, R. B., and A. G. Williamson. "Broadband design of coaxial line/rectangular waveguide probe transition." *Microwaves, Antennas and Propagation, IEE Proceedings*. Vol. 141. No. 1. IET, 1994.
- [12] Mehdi, Ghulam, Hu Anyong, and Miao Jungang. "A narrowband low noise amplifier for passive imaging systems." In *Applied Sciences and Technology (IBCAST)*, 2013 10th International Bhurban Conference on, pp. 455-458. IEEE, 2013.
- [13] Mehdi, Ghulam, Hu Anyong, and Miao Jungang. "Millimetre-wave all symmetric edge-coupled bandpass filter." In *Antennas, Propagation & EM Theory (ISAPE)*, 2012 10th International Symposium on, pp. 1271-1274. IEEE, 2012.
- [14] Yang, Baohua, Ghulam Mehdi, Anyong Hu, Yan Xie, Xianxun Yao, Jin Zhang, Cheng Zheng, and Jungang Miao. "The Round-Ended Design and Measurement of All Symmetric Edge-Coupled Bandpass Filter." *Progress In Electromagnetics Research C* 38 (2013): 191-203.
- [15] Riddle, Alf. "High performance parallel coupled microstrip filters." In *Microwave Symposium Digest*, 1988., IEEE MTT-S International, pp. 427-430. IEEE, 1988.
- [16] Kajfez, D., and S. Govind. "Effect of difference in odd-and even-mode wavelengths on a parallel-coupled bandpass filter." *Electronics Letters* 11, no. 5 (1975): 117-118.
- [17] Chang, C-Y., and Tatsuo Itoh. "A modified parallel-coupled filter structure that improves the upper stopband rejection and response symmetry." *Microwave Theory and Techniques, IEEE Transactions on* 39, no. 2 (1991): 310-314.
- [18] Riddle, Alf. "High performance parallel coupled microstrip filters." In *Microwave Symposium Digest*, 1988. IEEE MTT-S International, pp. 427-430. IEEE, 1988.
- [19] Matsuo, M., H. Yabuki, and M. Makimoto. "The design of a half-wavelength resonator BPF with attenuation poles at desired frequencies." In *Microwave Symposium Digest*. 2000 IEEE MTT-S International, vol. 2, pp. 1181-1184. IEEE, 2000.
- [20] Moradian, Mahdi, and Majid Tayarani. "Spurious-response suppression in microstrip parallel-coupled bandpass filters by grooved substrates." *Microwave Theory and Techniques, IEEE Transactions on* 56, no. 7 (2008): 1707-1713.
- [21] Soh, Johnson, Siou Teck Chew, and Ban Leong Ooi. "Parallel-coupled bandpass filter with improved rejection slope using δ -offset length." *Microwave and Optical Technology Letters* 50.3 (2008): 680-683.
- [22] Lee, Hong-Ming, and Chih-Ming Tsai. "Improved coupled-microstrip filter design using effective even-mode and odd-mode characteristic impedances." *Microwave Theory and Techniques, IEEE Transactions on* 53, no. 9 (2005): 2812-2818.
- [23] D. M. Pozar, *Microwave Engineering*, 2nd ed. New York: Wiley, 1998.

Ghulam Mehdi received his Bachelor of Engineering degree from NED University Karachi, Pakistan and Master of Engineering from Linkoping University, Linkoping, Sweden in 2000 and 2007 respectively. Currently, he is pursuing his PhD degree at Beijing University of Aeronautics and Astronautics University, Beijing, China. His research interest includes microwave and millimeter-wave circuit design.

Hu Anyong received his Bachelor of Engineering degree from the National University of Defence Technology, Changsha, China, in 2003. He got the PhD degree from Beijing University of Aeronautics and Astronautics (BUAA), Beijing, China, in 2009. Currently, he is faculty member at SOE&IE, BUAA, Beijing, China. His research interest includes signal processing, microwave remote sensing and microwave circuit design.

Jungang Miao received the B.S.E.E. degree from the National University of Defence Technology, Changsha, China, in 1982, the M.S.E.E. Degree from Beijing University of Aeronautics and Astronautics (BUAA), Beijing, China, in 1987, and the Dr. rer. nat. Degree in Physics from the University of Bremen, Germany, in 1998. From 1982 to 1984, Dr. Miao was working in Beijing with the Institute of Remote Sensing Instrumentation, Chinese Aerospace, where he developed space-borne micro-wave remote sensing instruments. From 1984 to 1993, he worked at the Electromagnetic Laboratory of BUAA, doing research and teaching in the field of microwave remote sensing. In 1993, he joined Institute of Environmental Physics and Remote Sensing, University of Bremen, Germany, as a staff member doing researches on space-borne microwave radiometry. In October 2003 he returned to the BUAA and since then he has been taking the Chair Professor position at the Electromagnetic Laboratory of BUAA. Dr. Miao's research areas include electromagnetic theory, microwave engineering and microwave remote sensing of the atmosphere, including sensor development, calibration and data analyses.